Available online at www.sciencedirect.com
ScienceDirect
Trans. Nonferrous Met. Soc. China 32(2022) 1050−1060
Transactions of Nonferrous Metals Society of China
www.tnmsc.cn

Electrochemical nucleation and growth of aluminum nanoparticles and leaf-like flat microstructures from reline deep eutectic solvent: Effect of temperature and angular speed of working electrode

G. VIDAL-GARCÍA[1], C. E. GUINTO-PANO[1], I. GARCÍA-HERNÁNDEZ[1], E. RODRÍGUEZ-CLEMENTE[1], P. MORALES-GIL[2], M. T. RAMÍREZ-SILVA[3], M. ROMERO-ROMO[1], M. PALOMAR-PARDAVÉ[1]

1. Universidad Autónoma Metropolitana-Azcapotzalco, Departamento de Materiales, Av. San Pablo 180 Col. Reynosa-Tamaulipas, CDMX, C.P. 02200, México;
2. Instituto Mexicano del Petróleo, Laboratorio de Caracterización de Materiales Sintéticos y Naturales, Eje Central Lázaro Cárdenas 152, CDMX, C.P. 07730, México;
3. Universidad Autónoma Metropolitana-Iztapalapa, Departamento de Química, Av. San Rafael Atlixco #186, Col. Vicentina, CDMX. C.P. 09340, México

Received 19 February 2021; accepted 3 November 2021

Abstract: The main objective of this work was to use reline deep eutectic solvent, containing Al(III) ions, for the electrochemical study of the nucleation and growth of aluminum onto a glassy carbon electrode at different temperatures and angular speeds (ω) of the working electrode. In order to fulfill this, electrochemical and surface characterization techniques were used. It was found that as temperature increased, the onset of the $Al(III)_{DES}$ reduction occurred at less negative potentials while the current peak of the voltammograms increased. These indicate that Al deposition thermodynamics and kinetics were favored. Practically, no anodic current was detected due to Al passivation by $Al(OH)_3$(s) and γ-Al_2O_3(s). At ω=0 r/min, the Al deposition chronoamperograms were analyzed by a theoretical model comprising Al 3D diffusion-controlled nucleation and growth and residual water reduction. However, those recorded at different angular speeds were analyzed with a theoretical model where adsorption−desorption and diffusion-controlled nucleation−growth occurred simultaneously. The deposits were characterized by SEM, EDX, XPS and XRD. At ω=0 r/min, formation of well distributed nanoparticles ((78.1±9.5) nm) was observed, while at ω=900 r/min the deposit was formed by multiple 10 μm diameter leaf-like flat microstructures, composed by Al, $Al(OH)_3$(s) and γ-A_2O_3(s).

Key words: aluminum; electrochemical nucleation; deep eutectic solvent; angular speed of working electrode; temperature

1 Introduction

The electrocatalytic properties of Al_2O_3 nano-coatings (both nanoparticles [1] and nano sheets [2]) onto carbon base electrodes, namely glassy carbon [1] and carbon paste [2], have been shown to be useful towards the oxidation of phenolic compounds (catecho, dopamine and tert-butylhydroquinone) [1] and alizarin [2]. Furthermore, it has been confirmed that Al_2O_3 can be used as an effective catalyst for the ozonation of refractory organic compounds (namely oxalic acid, acetic acid, salicylic acid and succinic acid) to CO_2 in aqueous solution [3], for mechanical and thermal stabilization of hybrid natural composites [4] and for the immobilization of *Kluyveromyces lactis* β-galactosidase on a bioaffinity support, concanavalin

Corresponding author: M. PALOMAR-PARDAVÉ, E-mail: mepp@correo.azc.uam.mx
DOI: 10.1016/S1003-6326(22)65854-0

A layered Al_2O_3 nanoparticles as biosensor applications [5]. In order to synthetize Al-based nanoparticles (namely Al_2O_3, Al and Al@$Al(OH)_3$), different methods were proposed: (1) chemical, through reduction of aluminum nitrate using citric acid [1] or a plant extract [4], (2) sonochemical, by sonication of aluminum isopropoxide, toluene and oleic acid mixture [6], (3) sol−gel by the hydrolysis of aluminum nitrate in twice-distilled urea water solutions at 100 °C [2], and (4) electrochemical deposition [7−22] using different ionic liquids, namely 1-butyl-3-methylimidazolium chloride [7] 1-butyl-1-methyl pyrrolidinium bis(trifluoromethyl-sulfonyl)imide saturated with $AlCl_3$ [8,9], 1-ethyl-3-methylimidazolium chloride: aluminium chloride [9−11], ($AlCl_3$)-trimethylphenylammonium chloride [12], $AlCl_3$ and $LiAlH_4$ in tetrahydro-furan [13], 3-butyl-1-ethylimidazolium tetrachloro-aluminate [14], $AlCl_3$−NaCl melts [15,16] and the so-called deep eutectic solvent (DES), developed by ABBOT et al [17,19], like the eutectic mixture of aluminum chloride and urea [20,21] and reline (eutectic mixture formed by choline chloride:urea) [22]. DES is akin to ionic liquids with the added advantages of being less toxic, cheaper and easier to prepare than the traditional ones.

In general, non-electrochemical methods require a series of time-consuming and costly stages and the resulting nanoparticles are obtained as a powder or are dispersed in a solvent. Contrary to that, when electrochemical means are used, the nanoparticles are deposited directly onto the final support in a single step. Recently, we have shown that the reline deep eutectic solvent, at 323 K and under stagnant conditions, can be used for the potentiostatic electrodeposition of Al@$Al(OH)_3$ nanoparticles onto a glassy carbon electrode and that the Al@$Al(OH)_3$ electrodeposition was attained directly from Al(III) ions that formed metallic Al, of which the nuclei provoked, in turn, residual water reduction on their growing surfaces [22]. Consequently, hydroxide ions formed and reacted with Al(III) ions in the DES, originating thus insoluble $Al(OH)_3$ onto the Al nuclei surfaces. In this work, we consider the effect of temperature and angular speed of the working electrode, which, to the best of our knowledge, have not been taken into consideration, on the kinetics of aluminum nucleation and growth from DES.

2 Experimental

2.1 Reline and Al(III) solution preparation

The reline deep eutectic solvent (DES), was prepared by mixing choline chloride and urea in a 1:2 molar ratio at 362 K following the experimental details as described elsewhere [21]. The previously dehydrated $AlCl_3·6H_2O$ salt, acquired from Meyer®, with purity ≥99.5%, was dissolved in the DES stirring for 12 h, thus becoming the electrolyte solution, while the DES without aluminum ions is termed the blank. All reagents were in analytical grade from Sigma-Aldrich. The water content of the DES was determined by Karl Fischer coulometric titration using a Titrino Coulometer model 756 from Metrohm® giving less than 0.15%.

2.2 Electrochemical study

A three electrode−electrochemical glass cell was used. The working electrode was a glassy carbon electrode (GCE), with an exposed area of 0.0706 cm^2, the counter electrode was a Pt wire, and a silver wire was used as quasi reference electrode (Ag QRE). The aluminum nucleation and growth mechanism onto the GCE was explored through electrochemical tests such as cyclic voltammetry (CV) and chronoamperometry (CA), in the reline eutectic mixture, containing 50 mmol/L $AlCl_3$. The CV and CA tests were carried out with a potentiostat−galvanostat PAR 263A−1, coupled to a PC running the Electrochemistry PowerSuite 2.56 software for data acquisition and experimental control. Different angular speeds of the working electrode were attained by means of a rotating GCE disk (GC-RDE), having a surface area of 0.1963 cm^2, connected to a rotation rate controller MSRX Speed Control, Analytical Rotator, Model AFMSRX, both from Pine Instruments Company.

The cell temperature was varied with the aid of a Lauda RMS circulator with RM6 refrigerating water bath chiller, from −15 to 100 °C, with temperature stability of ±0.02 °C. Before each experiment, the GCE surfaces were polished with diamond spray down to 0.25 μm, sonicated in methanol for 30 min, and finally rinsed with acetone to remove residual contaminants. All the electrochemical experiments were performed under N_2(g) atmosphere, previously dried through a pyrogallol trap.

2.3 SEM characterization

The morphology of the aluminum electrodeposits was characterized by scanning electron microscopy (SEM) using the Zeiss Supra 55VP electron microscope.

2.4 XPS analysis

The composition of the aluminum electrodeposit was determined by X-ray photoelectron spectroscopy (XPS) measurements, performed in an Escalab 250 Thermo Scientific equipment (base pressure ~2×10^{-7} Pa) with an Al filament emitting X-ray at 1486.6 keV. Fitting the XPS profiles was undertaken using the Avantage 5 software. Gaussian−Lorentzian (GL) line shape functions were employed, calibrated by assigning a binding energy (BE) value of 285 eV to the C 1s.

2.5 XRD characterization

XRD characterization of the aluminum electrodeposited on the GCE−RDE was carried out using a Bruker D8 Advance Series 2 diffractometer, equipped with a copper X-ray source and a scintillation detector, with a configuration θ–θ and radiation K_α (λ_{Cu}=0.15406 nm), scanning at 1.0 (°)/min in the range of 2θ=20°−80°.

3 Results and discussion

3.1 Effect of temperature

3.1.1 Potentiodynamic results

Figure 1 depicts a family of cyclic voltammograms, CVs, recorded during Al electrodeposition from reline onto the GCE surface, at a set potential scan rate, but varying the temperature of the electrolytic media. As the temperature increased, it is possible to note during the cathodic scan, that the onset of the $Al(III)_{DES}$ reduction process ($Al(III)_{DES}+3e=Al(0)_{GCE}$) occurs at a less negative potential while the corresponding current density peak, J_{cp}, becomes higher. These features strongly suggest that raising the temperature of the system favors both the thermodynamics and kinetics of this electrodeposition process. In all cases, during the anodic scan, the current was practically null due to passivation of the Al electrodeposited from the $Al(OH)_3(s)$ formed by the reaction of Al(III) ions in the DES and the hydroxyl ions generated by the concomitant reduction of the residual water in the DES ($2H_2O_{DES}+2e_{(Al)} \rightarrow H_{2(g)}+2OH^-_{DES}$) on the growing surfaces of the Al electrodeposit [22].

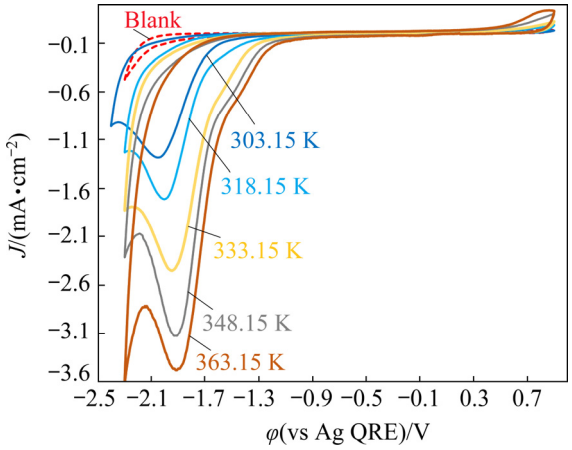

Fig. 1 CVs obtained in system of GCE/50 mmol/L Al(III) in reline DES at different temperatures (In all cases, the potential sweep started at 0.84 V, in the cathodic direction, at 50 mV/s)

As shown in Fig. 2(a), the absolute value of J_{cp} of the CVs recorded at 363.15 K, increases as a function of the applied potential scan rate, v. Furthermore, Fig. 2(b) depicts that J_{cp} depends linearly on v square root for all the temperatures considered in this work (the corresponding CVs are reported in Fig. S1 of the supporting material of this work), as predicted by the Berzins−Delahay equation (see Eq. (1)) [23]. This suggests that, regardless of the temperatures, aluminum deposition from the reline DES is a diffusion-controlled process. From the slope values of the regression lines reported in the inset of Fig. 2, (see Table S1 in the supporting information), and Eq. (1), one may calculate the diffusion coefficient of the Al(III) ions in these media, $D^{B-D}_{Al(III)}$, as a function of temperature, T. However, it is important to stress that Eq. (1) was derived under the consideration that the current density was due solely to the metal ion reduction on the electrode surfaces, which is not the case in the present system, where the water reduction reaction also contributes to the total current density.

$$J_{cp}=\frac{0.6105(zF)^{3/2}CD^{1/2}}{(RT)^{1/2}}v^{1/2} \quad (1)$$

where z is the total number of electrons transferred during the overall electrochemical process, F is the Faraday constant, T is the thermodynamic temperature (K), R is the molar gas constant ($J\cdot mol^{-1}\cdot K^{-1}$), C is the Al(III) bulk concentration ($mol\cdot cm^{-3}$), D is the diffusion coefficient of Al(III)

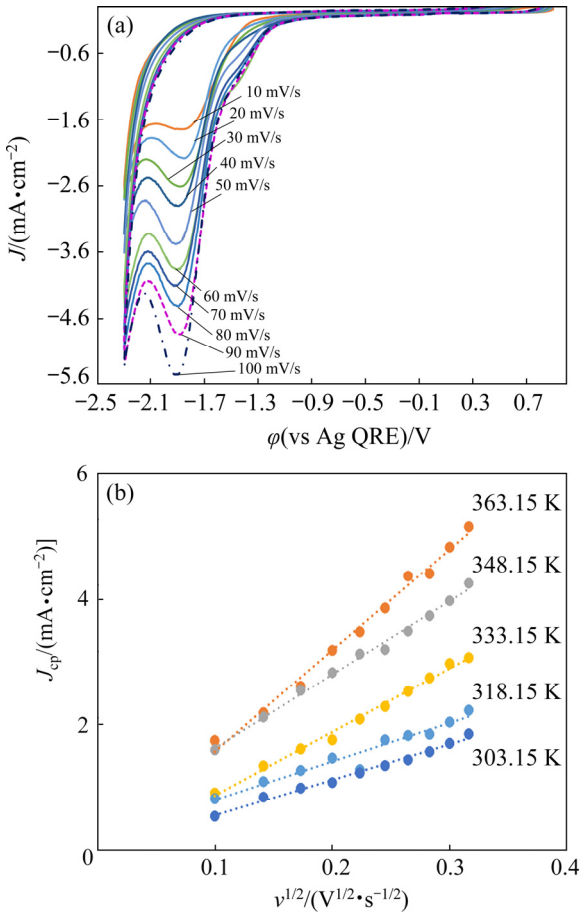

Fig. 2 CVs recorded in system of GCE/50 mmol/L Al(III) in reline DES at 363.15 K and different potential sweep rates (a), and J_{cp} vs $v^{1/2}$ plots of CVs recorded at different temperatures (b)

ions in reline DES ($cm^2 \cdot s^{-1}$), and v is the potential sweep rate (V/s).

Notwithstanding, for the sake of comparison, we have estimated $D_{Al(III)}^{B-D}$ as a function of T (see Fig. S2(a)). Furthermore, from the slope of the linear fitting of the equation to the experimental data in Fig. S2(b) and from the Arrhenius Eq. (2) [24,25], it was possible to estimate the activation energy for bulk diffusion, E_{bd}, of the aluminum ions in this medium as E_{bd}=39.59 kJ/mol.

$$\frac{\partial \ln D}{\partial(1/T)} = -\frac{E_{bd}}{R} \quad (2)$$

3.1.2 Potentiostatic result

Figure 3 shows a family of potentiostatic current density transients recorded during aluminum electrodeposition from reline DES at different temperatures, but at a fixed applied potential. All these $J-t$ plots depict the characteristic features corresponding to multiple diffusion-controlled 3D nucleation and growth of new phases on the electrode surfaces from residual water-containing DES, described in our previous works, namely, during Ni [26], Cr [27], Fe [28], Pd [29] and Al [22] electrodeposition. Therefore, they were analyzed with the same model described in these works [22,26−29], as shown in the supporting material.

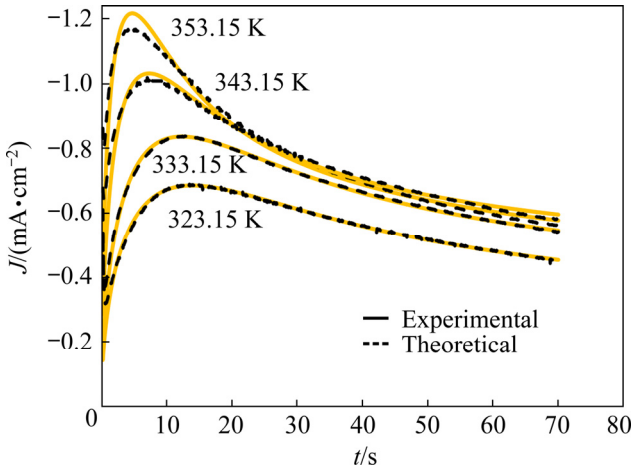

Fig. 3 Comparison between experimental potentiostatic current density transients, recorded in system of GCE/50 mmol/L $AlCl_3$ in reline DES, at −1.65 V, and different temperatures, with theoretical ones obtained after fitting Eqn. (S2) to experimental data

From this analysis, it was possible to estimate the best-fit parameters reported in Table S2 and to deconvolve the total current density of these plots in terms of their individual contributions, namely the 3D nucleation and diffusion controlled-growth, $J_{3D}(t)$, of aluminum centers and $J_{WR}(t)$, resulting from the residual water reduction on the growing surfaces of these aluminum nuclei, see Fig. S3. Moreover, this analysis allows to determine the nucleation rate, A, and the diffusion coefficient, D, of the Al(III) ions in these media as a function of temperature (see Figs. 4(a, b), respectively). It is possible to note that both depend exponentially on the temperature of the system (see Figs. S4(a) and S4(b)). In comparison, the D values estimated from the analysis of the potentiostatic current density transients (see Fig. 4(b)) are one order of magnitude lower than those assessed from analysis of the CV plots (see Fig. S2(a)). This difference is due to the unavoidable contribution of the water reduction to the current density measured from the CVs, while the current density transients $J_{3D}(t)$, used to evaluate

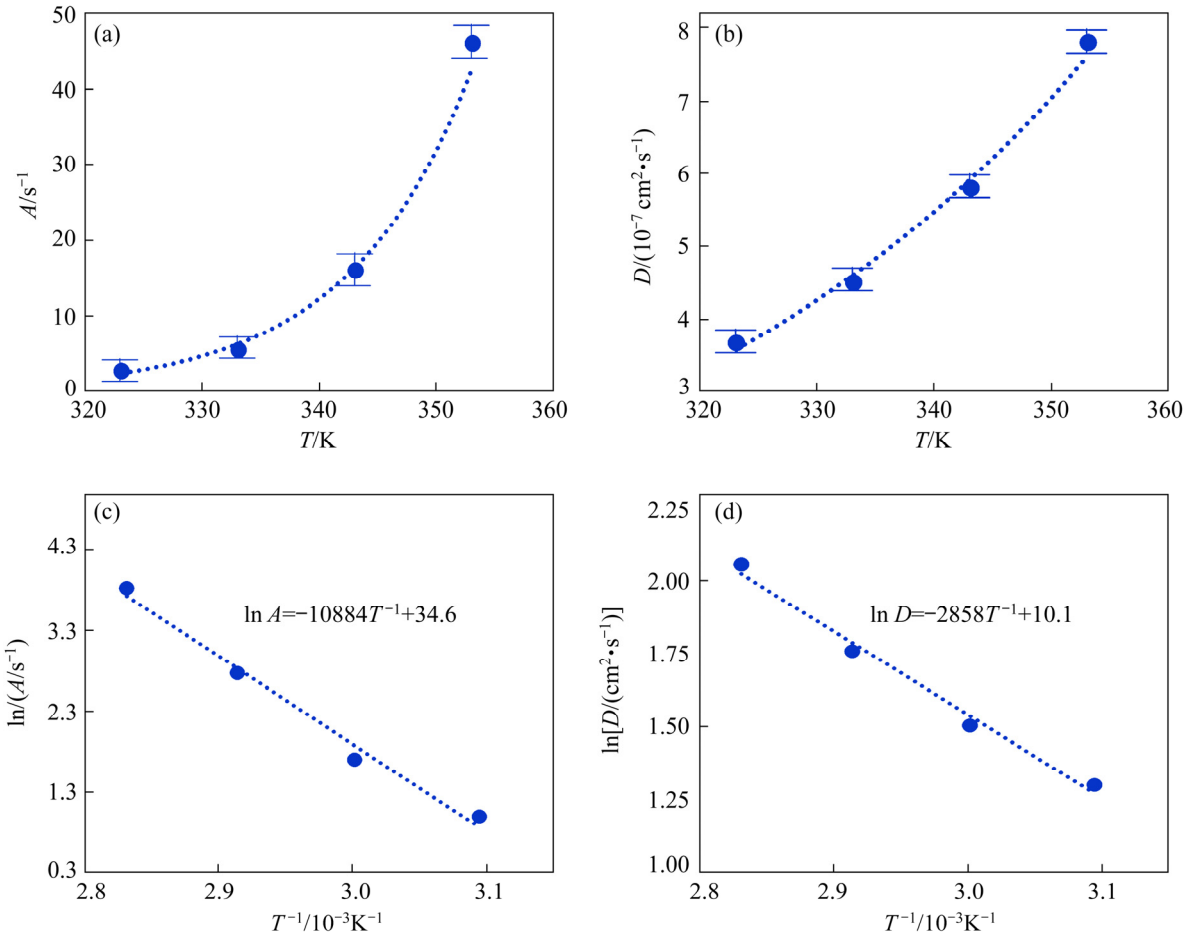

Fig. 4 Temperature dependence of aluminum nucleation frequency (A) (a) and Al(III) ion diffusion coefficient (D) (b); Arrhenius type plots of A (c) and D (d)

D (see Fig. S3) are all free from this contribution, and thus the D values reported in Table S1 are indeed reliable. From Arrhenius-type plots of A and D reported in Figs. 4(c, d), respectively, and Eqs. (2) and (3), the activation energy for Al nucleation, $E_{\text{nucleation}}$, and for bulk diffusion, E_{bd}, of the aluminum ions in this medium were calculated to be 90.5 and 23.8 kJ/mol, respectively.

$$\frac{\partial \ln A}{\partial(1/T)}=-\frac{E_{\text{nucleation}}}{R} \tag{3}$$

3.2 Effect of angular speed of working electrode

3.2.1 Potentiodynamic results

Figure 5(a) depicts a family of linear sweep voltammetry plots recorded at fixed temperature and potential sweep rate but varying the angular speed of the working electrode (GC−RDE). From Fig. 5(b), it is possible to note that the steady state current density increases as a function of the angular speed rate, as described by the Levich Eq. (4) [30]:

$$J_l=B\omega^{1/2} \tag{4}$$

with

$$B=0.620zFD^{2/3}\upsilon^{-1/6}C \tag{5}$$

where J_l is the limiting current density, ω is angular speed of the electrode (rad/s), and υ is the kinematic viscosity. To use the equation as written above (with the leading 0.620), radians per second for angular rotation units must be used. If revolutions (rotation) per minute is used, a value of 0.201 should be used in place of 0.620.

3.2.2 Potentiostatic results

Figure 6 shows a family of experimental potentiostatic current density transients recorded during Al electrodeposition at a fixed temperature and applied potential but different angular speeds of the working electrode. The shape of these plots (monotonically rising transients, followed by convergence to a limiting current that follows the

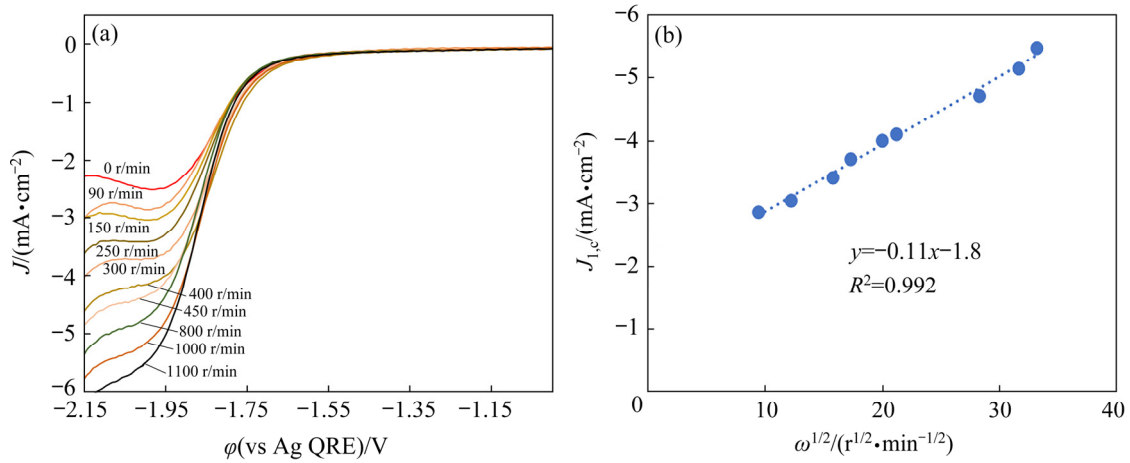

Fig. 5 Linear sweep voltammograms recorded in system of GC−RDE/50 mmol/L Al (III) in reline DES at 80 mV/s, 333.15 K and different electrode angular speeds, ω (a), and $J_{l,c}$ vs $\omega^{1/2}$ plot of CVs recorded at −2.0 V (b)

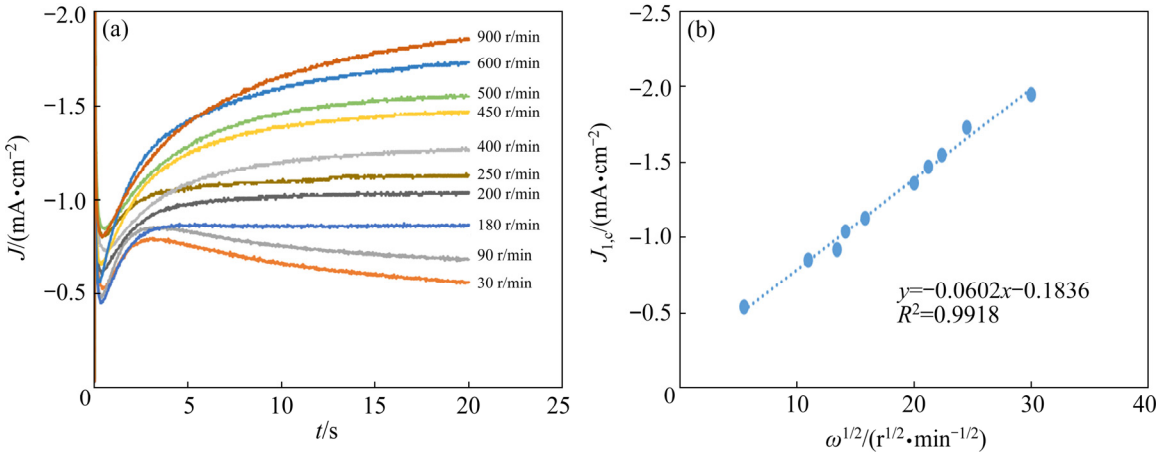

Fig. 6 J–t plots recorded in system of GC−RDE/50 mmol/L Al (III) in reline DES at −2.0 V, 333.15 K and different ω (a), and $J_{l,c}$ plots of system recorded at 20 s as function of $\omega^{1/2}$ (b)

Levich equation (5), see Fig. 6(b)) are indeed quite similar to the theoretical model reported by HYDE et al [31,32], to describe the diffusion controlled nucleation of hemispherical centers under different angular speeds of the working electrode (see Eq. (6)). However, a current spike due to a pseudo-capacitance process, can be clearly seen, in all cases, before the rising zone of the transients. This adsorption (desorption) process of chemical species constituting this electrolytic bath which could be adsorbed (desorbed), namely chloride ions and aluminum chloride complex, $Al(Cl)_n^{3-n}$, taking place parallel to a nucleation and growth process, has been modeled as Eq. (7) by HÖLZLE et al [33]:

$$J_{\text{dc-fcon}}(t) = R[1-\exp(-Qt^{1/2}\{1-\exp(-At)\cdot [1+\frac{At}{3}+\frac{(At)^2}{10}+\frac{(At)^3}{42}]\})] + J_0 \quad (6)$$

with

$$Q = 2\sqrt{2\pi}\left(\frac{MC}{\rho}\right)^{1/2} D^{1/2}\delta N_0 \quad (7)$$

$$R = zF\frac{DC}{\delta} \quad (8)$$

where M and ρ are the molecular mass and the deposit density, respectively, N_0 is the number density of active sites available for the nucleation process on the substrate surface, A is the nucleation frequency, δ is the diffusion layer thickness, and J_0 is the current offset.

$$J_{\text{ad}}(t) = k_1\exp(-k_2 t) \quad (9)$$

with

$$k_1 = \frac{\varphi}{R_s} \quad (10)$$

$$k_2 = \frac{1}{R_s C_{\text{pc}}} \quad (11)$$

where φ is the applied potential, R_s is the solution's resistance and C_{pc} is a pseudo-capacitance.

Considering these features, we propose that the plots in Fig. 6(a) can be described by adding Eqs. (6) and (9) as follows:

$$J(t) = J_{ad}(t) + J_{dc\text{-}fcon}(t) \quad (12)$$

Figure 7 shows a comparison of some of the $J-t$ plots reported in Fig. 6(a) with theoretical ones, generated by non-linear fit of Eq. (12). It can be seen that this model describes quite well the experimental evidence. From this analysis (see Table S3), it can be noted that at constant temperature and applied potential, the nucleation frequency of Al(0) increases exponentially with the electrode rotation rate while the parameters k_1 and k_2 associated with adsorption (desorption) processes of Cl^- and $Al(Cl)_n^{3-n}$ species that form the electrolytic bath, are practically independent of ω as expected from an adsorption−desorption process.

3.3 SEM, EDX, XPS and XRD analysis results

Figure 8 depicts a comparison of SEM images obtained on the GC−RDE surfaces electrodeposited

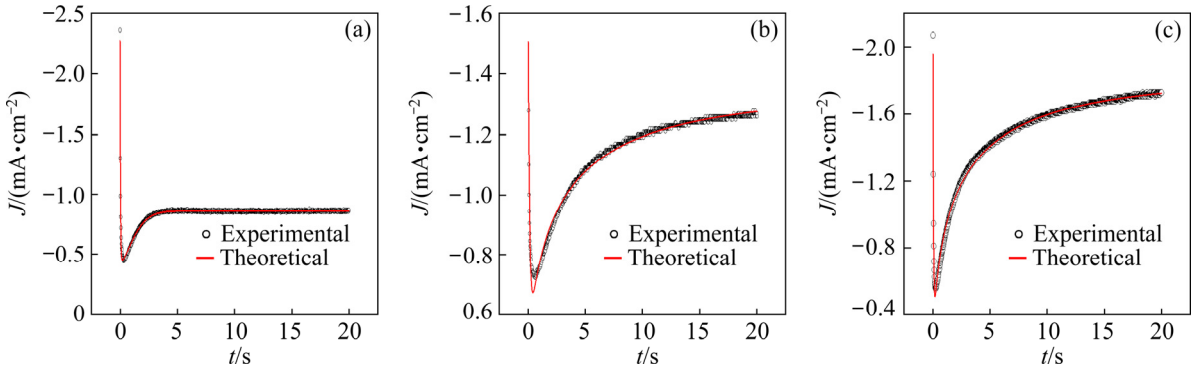

Fig. 7 Comparison of experimental $J-t$ plots reported in Fig. 6(a) for 200 (a), 450 (b) and 900 r/min (c) with theoretical ones obtained by non-linear fit of Eq. (12) to experimental data

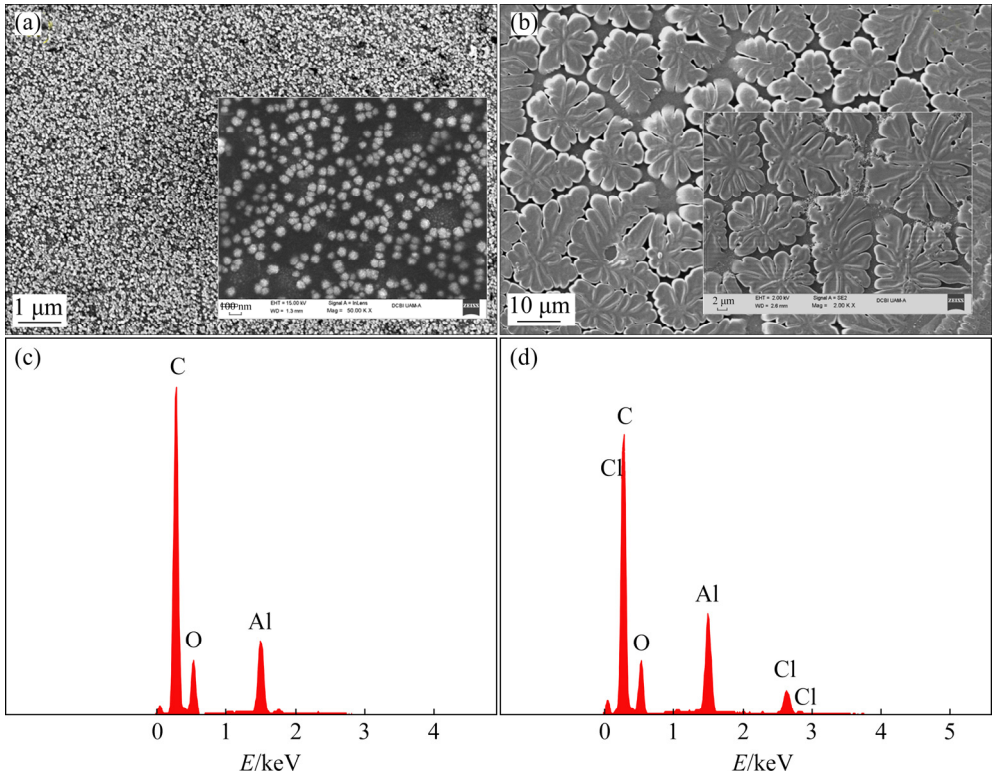

Fig. 8 SEM images (a, b) and corresponding EDX spectra (c, d) recorded on surface of GC−RDE after potentiostatic (−2.0 V) electrodeposition of Al during 100 s, from reline containing 50 mmol/L Al(III) at 333.15 K and different angular speeds: (a, c) 0; (b, d) 900 r/min (The insets in the SEM images correspond to higher magnification images)

with aluminum (see Reactions (R1)−(R4) in the supporting material of this work), from the reline DES, under stagnant (0 r/min) conditions (Fig. 8(a)), and at an angular speed of the working electrode of 900 r/min (Fig. 8(b)), but keeping the same temperature and applied potential. At 0 r/min, the formation of well distributed nanoparticles ((78.1±9.5) nm) (see Fig. S6) can be seen, while at 900 r/min, the deposit is formed by multiple leaf-like flat microstructures of about 10 μm in diameter composed by Al and O in both cases. To the best of our knowledge, this is the first time that the latter Al structures are reported prepared by means of electrodeposition. When a slower angular velocity was imposed to the CG−RDE, the deposit was formed by a mix of nanoparticles and leaf-like flat microstructures (see Fig. S7(a)). Meanwhile, when the temperature of the DES was reached (at the same angular velocity and applied potential), the presence of blisters was notorious (see Figs. S7(b) and S7(c)), most probably due to intense hydrogen evolution of which the reaction rate is favored at higher temperature (see Fig. S5(b)) for instance.

In order to further determine the nature of the leaf-like flat microstructures recorded at 900 r/min (under stagnant conditions determined elsewhere [22]), XPS analysis was carried out on the surfaces of the sample reported in Fig. 8(b). From Fig. 9, it is possible to note that these surfaces contain two expected elements, Al (see Fig. 9(a)) in two oxidation states: (III) and zero, and O (see Fig. 9(b)). The latter is quite similar to that reported and analyzed for γ-alumina nanosheets [2], which conclusively proves the presence of AlO_x−OH_y hydroxyl/hydroxide groups on its surface, besides the Al_2O_3. Thus, it can be concluded that the leaf-like flat microstructures were formed by Al, Al_2O_3 and AlO_x−OH_y. Furthermore, from XRD analysis (see Fig. 9(c)), it is also possible to note the presence of metallic aluminum [34], $Al(OH)_3$ [35] and γ-Al_2O_3 [2,36] which were formed according to the reaction mechanism reported in the supporting material (see Reactions (R1)−(R4)) and schematically described in Fig. 10.

4 Conclusions

(1) The increase in the temperature of the electrolytic bath used favored the thermodynamics and kinetics of the aluminum electrodeposition process.

(2) The different angular speeds of the working electrode considered, directly impacted the aluminum deposit morphology: nanoparticles under stagnant conditions and leaf-like forms at 900 r/min.

(3) From J−t plots, it was demonstrated that under stagnant conditions, aluminum electrodeposition is a 3D nucleation and diffusion-controlled process with growth of a new phase, $Al(OH)_{3(s)}$ and γ-Al_2O_3(s) on the Al(0) nuclei surface due to DES residual water reduction.

(4) At different angular speeds of the working electrode, two processes occurred simultaneously: adsorption-desorption and diffusion-controlled nucleation−growth.

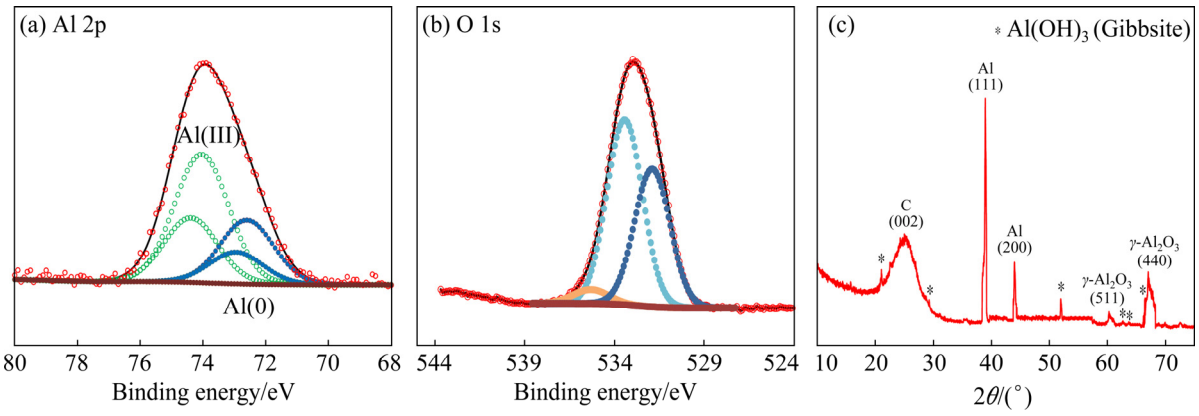

Fig. 9 Experimental XPS spectra carried out on surface of GC−RDE electrodeposited with leaf-like flat microstructures ((a) Al 2p; (b) High resolution O 1s spectrum) and XRD pattern of Al electrodeposited on GCE−RDE recorded after potentiostatic (−2.0 V) electrodeposition of Al during 5 h, from reline DES containing 50 mmol/L Al(III) at 333.15 K and 900 r/min (c)

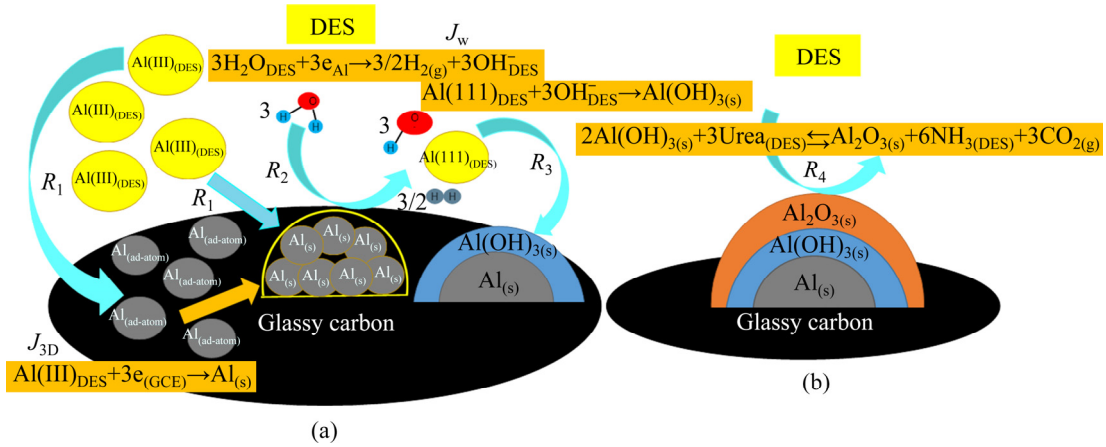

Fig. 10 Reaction mechanism involved during Al potentiostatic electrodeposition from reline DES (a) and plausible explanation of formation of γ-Al_2O_3 on surfaces of Al@$Al(OH)_3$ electrodeposit by interaction of $Al(OH)_3$ with urea (see Reaction (R4) in supporting material) (b)

Supporting materials

The supporting materials in this work can be found at: http://www.ysxbcn.com/download/TNMSC-2022-p1050.pdf.

Acknowledgments

G. VIDAL-GARCÍA thanks CONACyT for the scholarship granted to pursue postgraduate studies. The authors like to thank CONACyT for Project 258487. E. RODRÍGUEZ-CLEMENTE thanks CONACyT for the support given to undertake a postdoctoral stay through Project 258487. E. RODRÍGUEZ-CLEMENTE, M. ROMERO-ROMO, M. T. RAMÍREZ-SILVA, P. MORALES-GIL and M. PALOMAR-PARDAVÉ wish to thank the SNI for the distinction of their membership and the stipend received. The authors are indebted to Dra. Deyanira ÁNGELES-BELTRÁN (Laboratorio de Microscopía Electrónica de la División de CBI) and Dra. Leticia JUÁREZ-MARMOLEJO for the SEM images and their analysis, respectively.

References

[1] LIMA A P, SOUZA R C, SILVA M N T, GONÇALVES R F, NOSSOL E, RICHTER E M, LIMA R C, MUNOZ R A A. Influence of Al_2O_3 nanoparticles structure immobilized upon glassy-carbon electrode on the electrocatalytic oxidation of phenolic compounds [J]. Sensors and Actuators B, 2018, 262: 646−654.

[2] MA Chuan-li, CHANG Yan-long, YE Wei-chun, SHANG Wei, WANG Chun-ming. Supercritical preparation of hexagonal γ-alumina nanosheets and its electrocatalytic properties [J]. Journal of Colloid and Interface Science, 2008, 317: 148−154.

[3] ERNST M, LUROT F, SCHROTTER J C. Catalytic ozonation of refractory organic model compounds in aqueous solution by aluminum oxide [J]. Applied Catalysis B: Environmental, 2004, 47: 15−25.

[4] SUMESH K R, KANTHAVEL K. Green synthesis of aluminium oxide nanoparticles and its applications in mechanical and thermal stability of hybrid natural composites [J]. Journal of Polymers and the Environment, 2019, 27: 2189−2200.

[5] ANSARI S A, HUSAIN Q. Immobilization of Kluyveromyces lactis galactosidase on concanavalin A layered aluminium oxide nanoparticles—Its future aspects in biosensor applications [J]. Journal of Molecular Catalysis B: Enzymatic, 2011, 70: 119−126.

[6] SHABANA S, SONAWANE S H, RANGANATHAN V, PUJJALWAR P H, PINJARI D V, BHANVASE B A, GOGATED P R. MUTHUPANDIAN A. Improved synthesis of aluminium nanoparticles using ultrasound assisted approach and subsequent dispersion studies in di-octyl adipate [J]. Ultrasonics Sonochemistry, 2017, 36: 59−69.

[7] ZHANG D, MU Y G, LI H P, YANG Z G, YANG Y. A new method for electrodeposition of Al coatings from ionic liquids on AZ91D Mg alloy in air [J]. Royal Society of Chemistry Advances, 2018, 8: 39170−39176.

[8] ZEIN EL ABEDIN S, MOUSTAFA E M, HEMPELMANN R, NATTER H, ENDRES F. Additive free electrodeposition of nanocrystalline aluminium in a water and air stable ionic liquid [J]. Electrochemistry Communications, 2005, 7: 1111−1116.

[9] MOUSTAFA E M, ZEIN EL ABEDIN S, SHKURANKOV A, ZSCHIPPANG E, SAAD A Y, BUND A, ENDRES F. Electrodeposition of Al in 1-butyl-1-methylpyrrolidinium bis(trifluoromethylsulfonyl)amide and 1-ethyl-3-methylimidazolium bis(trifluoromethylsulfonyl)amide ionic liquids: In situ STM and EQCM studies [J]. Journal of Physical Chemistry B, 2007, 111: 4693−4704.

[10] PERRE E, NYHOLM L, GUSTAFSSON T, TABERNA P L, SIMON P, EDSTRÖM K. Direct electrodeposition of aluminium nano-rods [J]. Electrochemistry Communications, 2008, 10: 1467−1470.

[11] JIANG T, CHOLLIER BRYM M J, DUBÉ G, LASIA A, BRISARD G M. Electrodeposition of aluminium from ionic liquids: Part I—Electrodeposition and surface morphology of aluminium from aluminium chloride ($AlCl_3$)−1-ethyl-3-methylimidazolium chloride ([EMIm]Cl) ionic liquids [J]. Surface & Coatings Technology, 2006, 20: 1−9.

[12] JIANG T, CHOLLIER BRYM M J, DUBÉ G, LASIA A, BRISARD G M. Electrodeposition of aluminium from ionic liquids: Part II — Studies on the electrodeposition of aluminum from aluminum chloride ($AlCl_3$)-trimethylphenylammonium chloride (TMPAC) ionic liquids [J]. Surface & Coatings Technology, 2006, 20: 10−18.

[13] LEFEBVRE M C, CONWAY B E. Nucleation and morphologies in the process of electrocrystallization of aluminium on smooth gold and glassy-carbon substrates [J]. Journal of Electroanalytical Chemistry, 2000, 480: 46−58.

[14] GUINEA E, SALICIO-PAZ A, IRIARTE A, GRANDE H J, MEDINA E, GARCÍA-LECINA E. Robust aluminum electrodeposition from ionic liquid electrolytes containing light aromatic naphta as additive [J]. Chemistry Open, 2019, 8: 1094−1099.

[15] KAN H M, WANG Z W, WANG X Y, ZHANG N. Electrochemical deposition of aluminum on W electrode from $AlCl_3$−NaCl melts [J]. Transactions of Nonferrous Metals Society of China, 2010, 20: 158−164.

[16] LI Q, HJULER H A, BERG R W, BJERRUM N. Electrochemical deposition of aluminum from NaCl−$AlCl_3$ melts [J]. Journal of the Electrochemical Society, 1990, 137: 593−598.

[17] SMITH E L, ABBOTT A P, RYDER K S. Deep eutectic solvents (DESs) and their applications [J]. Chemical Reviews, 2014, 114(21): 11060−11082.

[18] YUE G K, ZHANG S J, ZHU Y L, LU X M, LI S C, LI Z X. A promising method for electrodeposition of aluminium on stainless steel in ionic liquid [J]. AlChE Journal, 2009, 55(3): 783−796.

[19] ABBOTT A P, QIU F, ABOOD H M A, ALI M R, RYDER K S. Double layer, diluent and anode effects upon the electrodeposition of aluminium from chloroaluminate based ionic liquids [J]. Physical Chemistry Chemical Physics, 2010, 12(8): 1862−1872.

[20] ABBOTT A P, HARRIS R C, HSIEH Y T, RYDER K S, SUN I W. Aluminium electrodeposition under ambient conditions [J]. Physical Chemistry Chemical Physics, 2014, 16: 14675−14681.

[21] CVETKOVIĆ V S, VUKIĆEVIĆ N M, JOVIĆEVIĆ N, STEVANOVIĆ J S, JOVIĆEVIĆ J N. Aluminium electrodeposition under novel conditions from $AlCl_3$−urea deep eutectic solvent at room temperature [J]. Transactions of Nonferrous Metals Society of China, 2020, 30: 823−834.

[22] RODRÍGUEZ-CLEMENTE E, MANH T L, GUINTO-PANO C E, ROMERO-ROMO M, MEJÍA-CABALLERO I, MORALES-GIL P, PALACIOS-GONZÁLEZ E, RAMÍREZ-SILVA M T, PALOMAR-PARDAVÉ M. Aluminum electrochemical nucleation and growth onto a glassy carbon electrode from a deep eutectic solvent [J]. Journal of the Electrochemical Society, 2019, 166: D3035−D3041.

[23] BERZINS T, DELAHAY P. Oscillographic polarographic waves for the reversible deposition of metals on solid electrodes [J]. Journal of the American Chemical Society, 1953, 75: 555−559.

[24] MOSTANY J, SCHARIFKER B R, SAAVEDRA K, BORRÁS C. Electrochemical nucleation and the classical theory: Overpotential and temperature dependence of the nucleation rate [J]. Russian Journal of Electrochemistry, 2008, 44: 652−658.

[25] PALOMAR-PARDAVÉ M, ALDANA-GONZÁLEZ J, BOTELLO L E, ARCE-ESTRADA E M, RAMÍREZ-SILVA M T, MOSTANY J, ROMERO-ROMO M. Influence of temperature on the thermodynamics and kinetics of cobalt electrochemical nucleation and growth [J]. Electrochimica Acta, 2017, 241: 162−169.

[26] ALDANA-GONZÁLEZ J, ROMERO-ROMO M, ROBLES-PERALTA J, MORALES-GIL P, PALACIOS-GONZÁLEZ E, RAMÍREZ-SILVA M T, MOSTANY J, PALOMAR-PARDAVÉ M. On the electrochemical formation of nickel nanoparticles onto glassy carbon from a deep eutectic solvent [J]. Electrochimica Acta, 2018, 276: 417−423.

[27] MEJÍA-CABALLERO I, ALDANA-GONZÁLEZ J, MANH T L, ROMERO-ROMO M, ARCE-ESTRADA E M, CAMPOS-SILVA I, RAMÍREZ-SILVA M T, PALOMAR-PARDAVÉ M. Mechanism and kinetics of chromium electrochemical nucleation and growth from a choline chloride/ethylene glycol deep eutectic solvent [J]. Journal of the Electrochemical Society, 2018, 165: D393−D401.

[28] PALOMAR-PARDAVÉ M, MOSTANY J, MUÑOZ-RIZO R, BOTELLO L E, ALDANA-GONZÁLEZ J, ARCE-ESTRADA E M, MONTES DE OCA-YEMHA M G, RAMÍREZ-SILVA M T, ROMERO-ROMO M. Electro-chemical study and physicochemical characterization of iron nanoparticles electrodeposited onto HOPG from Fe(III) ions dissolved in the choline chloride-urea deep eutectic solvent [J]. Journal of Electroanalytical Chemistry, 2019, 851: 113453.

[29] JUÁREZ-MARMOLEJO L, MALDONADO-TEODOCIO B, MONTES DE OCA-YEMHA M G, ROMERO-ROMO M, RAMÍREZ-SILVA M T, ARCE-ESTRADA E M, MORALES-GIL P, MOSTANY J, PALOMAR-PARDAVÉ M. Mechanism and kinetics of palladium nanoparticles electrochemical formation onto glassy carbon, from a deep eutectic solvent (Reline) [J]. Journal of Physical Chemistry B, 2020, 124: 3973−3983.

[30] BARD A J, FAULKNER L R. Electrochemical methods: Fundamentals and applications [M]. 2nd ed. New York: Wiley, 2000.

[31] HYDE M E, KLYMENKO O V, COMPTON R G. The theory of electrodeposition in the presence of forced convection: transport controlled nucleation of hemispheres [J]. Journal of Electroanalytical Chemistry, 2002, 534: 13−17

[32] HYDE M E, COMPTON R G. Theoretical and experimental aspects of electrodeposition under hydrodynamic conditions [J]. Journal of Electroanalytical Chemistry, 2005, 581: 224−230.

[33] HÖLZLE M H, RETTER U, KOLB D M. The kinetics of structural changes in Cu adlayers on Au(111) [J]. Journal of Electroanalytical Chemistry, 1994, 371: 101−109.
[34] LI M, LI Y. Aluminum electrodeposition using $AlCl_3$/urea ionic liquid [J]. International Journal of Electrochemical Science, 2020, 15: 8498−8505.
[35] SU S Q, YANG J, MA H M, JIANG F, LIU Y Q, LI G. Preparation of ultrafine aluminum hydroxide from coal fly ash by alkali dissolution process [J]. Integrated Ferroelectrics, 2011, 128: 155−162.
[36] LIAN J B, MA J M, DUAN X C, KIM T, LI H B, ZHENG W J. One- step ionothermal synthesis of γ-Al_2O_3 mesoporous nanoflakes at low temperature [J]. Chemical Communications, 2010, 46: 2650−2652.

Reline 低熔溶剂中铝纳米颗粒和叶状显微组织的电化学形核和长大：温度和工作电极角速度的影响

G. VIDAL-GARCÍA[1], C. E. GUINTO-PANO[1], I. GARCÍA-HERNÁNDEZ[1], E. RODRÍGUEZ-CLEMENTE[1], P. MORALES-GIL[2], M. T. RAMÍREZ-SILVA[3], M. ROMERO-ROMO[1], M. PALOMAR-PARDAVÉ[1]

1. Universidad Autónoma Metropolitana-Azcapotzalco, Departamento de Materiales, Av. San Pablo 180 Col. Reynosa-Tamaulipas, CDMX, C.P. 02200, México;
2. Instituto Mexicano del Petróleo, Laboratorio de Caracterización de Materiales Sintéticos y Naturales, Eje Central Lázaro Cárdenas 152, CDMX, C.P. 07730, México;
3. Universidad Autónoma Metropolitana-Iztapalapa, Departamento de Química, Av. San Rafael Atlixco #186, Col. Vicentina, CDMX. C.P. 09340, México

摘　要：利用电化学和表面表征技术，研究在不同温度和工作电极角速度(ω)下，含 Al(III)离子的 Reline 低共熔溶剂中铝在玻碳电极上形核和长大的电化学行为。结果表明，随着温度的升高，$Al(III)_{DES}$ 的还原发生在较低的负电位，而此时伏安图中的电流峰增大，这对 Al 沉积动力学和热力学条件有利。实际上，由于 Al 被 $Al(OH)_3$(s)和 Al_2O_3(s)钝化，未检测到阳极电流。当 ω=0 r/min 时，通过由 Al 三维扩散控制的形核、长大和残余水还原组成的理论模型，分析 Al 沉积时计时电流图。然而，用于分析不同角速度下的理论模型，其吸附−解吸和扩散控制的形核−长大是同时发生的。用 SEM、EDX、XPS 和 XRD 表征沉积物，结果表明，当 ω=0 r/min 时，形成分布良好的纳米颗粒((78.1±9.5) nm)；而当 ω=900 r/min 时，形成直径约为 10 μm，由 Al、$Al(OH)_3$(s)和 γ-A_2O_3(s)组成的叶状显微组织。

关键词：铝；电化学形核；低共熔溶剂；工作电极角速度；温度

(Edited by Bing YANG)